

# THE SIMULATION STUDY OF THE SINGLE BUNCH INSTABILITIES IN THE SPRING-8 STORAGE RING

Takeshi Nakamura, SPring-8, Kamigori, Ako-gun, Hyogo, Japan

## 1. INTRODUCTION

The simulation code for single-bunch instabilities, SISR(Single-Bunch Instabilities in Storage Rings) was developed and applied to study instabilities in the SPring-8 storage ring. SISR uses complex amplitude of betatron motion and it enable to treat both distributed broad-band impedance such as small discontinuities of a beam pipe and localized impedance like cavities.

## 2. EQUATIONS OF MOTION

The transverse motion of i-th electron under the force  $F$  is represented with  $\eta_i$  as

$$\eta_i = \frac{x_i}{\sqrt{\beta}}, \quad \theta = \frac{1}{v_0} \int^s \frac{ds'}{\beta} \quad (1)$$

$$\frac{d^2 \eta_i}{d\theta^2} + (v_0 + \Delta v_i)^2 \eta_i = v_0^2 \beta^{\frac{3}{2}} \frac{F_i}{E} \quad (2)$$

where  $v_0$ ,  $\beta$  and  $E$  is the betatron tune, the beta function and the energy, respectively.

The force  $F_i$  from wake field is

$$\begin{aligned} F_i &= e \sum_{j=1}^{N_p} q_j x_j \frac{d}{ds} W^\perp(z_j - z_i, s) \\ &= e \beta^{\frac{1}{2}} \sum_{j=1}^{N_p} q_j \eta_j \frac{d}{ds} W^\perp(z_j - z_i, s) \end{aligned} \quad (3)$$

Assuming that

$$\left| \frac{d^2 a_i}{d\theta^2} \right| \ll \left| 2 i v_0 \frac{da_i}{d\theta} \right| \quad (4)$$

, which means that the typical varying time of  $a_i$  is much smaller than the betatron period  $\lambda\beta/c$ , and using the phasers shown below,

$$\eta_i = \text{Re}[a_i(\theta) e^{i v_0 \theta}] = \frac{1}{2} (a_i(\theta) e^{i v_0 \theta} + c.c) \quad (5)$$

$$F_i = \text{Re}[f_i(\theta) e^{i v_0 \theta}] = \frac{1}{2} (f_i(\theta) e^{i v_0 \theta} + c.c) \quad (6)$$

$$f_i(\theta) = e \beta^{\frac{1}{2}} \sum_{j=1}^{N_p} q_j a_j \frac{d}{ds} W^\perp(z_j - z_i, s), \quad (7)$$

the equation (2) become

$$\begin{aligned} \frac{da_i}{d\theta} &= i \Delta v_i a_i + \frac{v_0}{2 i E_0} \int_{\theta - \frac{\pi}{2v_0}}^{\theta + \frac{\pi}{2v_0}} \beta^{\frac{3}{2}} f_i \left( \frac{d\theta'}{v_0} \right) \\ &\quad + \frac{v_0}{2 i E_0} \int_{\theta - \frac{\pi}{2v_0}}^{\theta + \frac{\pi}{2v_0}} \beta^{\frac{3}{2}} f_i e^{-2 i v_0 \theta'} \left( \frac{d\theta'}{v_0} \right) \end{aligned} \quad (8)$$

The third term of the right hand side can be set to zero in usual cases because  $\beta^{3/2} f$  usually does not have the Fourier component of the frequency  $2v_0$ .

Hence the equation

$$\frac{da_i}{d\theta} = i \Delta v_i a_i + \frac{v_0}{2 i E_0} \int_{\theta - \frac{\pi}{2v_0}}^{\theta + \frac{\pi}{2v_0}} \beta^{\frac{3}{2}} f_i \left( \frac{d\theta'}{v_0} \right) \quad (9)$$

is used to simulate distributed impedance.

The integral in this equation (9) can be written as

$$\int_{\theta - \frac{\pi}{2v_0}}^{\theta + \frac{\pi}{2v_0}} \beta^{\frac{3}{2}} f_i \left( \frac{d\theta'}{v_0} \right) = \int_{s - \frac{\lambda}{2}}^{s + \frac{\lambda}{2}} \beta^{\frac{1}{2}} f_i \frac{ds'}{2\pi} = \frac{1}{2\pi} \int_{s - \frac{C}{2}}^{s + \frac{C}{2}} \beta^{\frac{1}{2}} f_i ds' \frac{\lambda\beta}{C}$$

and from the approximation (4), we have

$$\begin{aligned} \int_{s - \frac{C}{2}}^{s + \frac{C}{2}} \beta^{\frac{1}{2}} f_i ds' &= \sum_k \beta_k^{\frac{1}{2}} \int_{k\text{th element}} f_i ds' \\ &= e \sum_k \beta_k \sum_j q_j a_j W_k^\perp(z_j - z_i) \\ &= e \sum_j q_j a_j \sum_k \beta_k W_k^\perp(z_j - z_i) \end{aligned}$$

and, from the definition of  $\lambda\beta$ ,  $\frac{\lambda\beta}{C} = \frac{1}{v_0}$ .

The final form of the equation of transverse motion of particles used in CISR is

$$\frac{da_i}{d\theta} = i \Delta v_i a_i + \frac{e}{4i\pi E_0} \sum_{j=1}^{N_p} q_j a_j \sum_{k=1}^{N_I} \beta_k W_k^\perp(z_j - z_i) \quad (10)$$

## 3. DIFFERENCE EQUATIONS

The difference equations used in CISR to simulate the electron motion are as follows. For longitudinal motion,  $\Delta E_i = E_i - E_0$  and  $z = s - ct$ , where  $s$  is the co-ordinate to the direction of particle, is used to describe longitudinal motion of particles.  $T_0$  and  $E_0$  are the revolution period and reference energy, respectively.

In the following, the symbol with superscript + and - are the value after and before the passage of each element. In the following, respectively.

### 3.1 Lattice with Distributed Broad-Band Impedance

$$\Delta E_i^+ = \Delta E_i^\pm \pm U_0 \frac{\Delta T}{T_0} \left( 1 + \frac{\Delta E_i^\pm}{E_0} \right)^2 \quad (11)$$

$$z_i^+ = z_i^\pm \pm \alpha \frac{\Delta E_i^\pm}{E_0} c \Delta T \quad (12)$$

$$r_i^+ = r_i^\pm + \text{Re} \left[ f_i^\pm e^{\pm i \phi_{i,n}} \right] \Delta \theta \quad (13)$$

$$\phi_i^+ = \phi_i^\pm + \Delta v_i \Delta \theta + \frac{\text{Im} \left[ g_i^\pm e^{\pm i \phi_i^\pm} \right]}{\left[ (r_i^+ + r_i^\pm) / 2 \right]} \Delta \theta \quad (14)$$

$$g_i^\pm = \frac{1}{4i\pi E_0} \sum_{j=1}^{N_p} q_j a_j^\pm \sum_{k=1}^{N_I} \beta_k W_k^\perp(z_j^\pm - z_i^\pm) \quad (15)$$

where  $\Delta\theta = 2\pi \frac{\Delta T}{T_0}$ ,  $r = |a|$ ,  $a = re^{i\phi}$ .

### 3.2 Localized Broad-Band Impedance

For the localized impedance such as cavities,

$$\Delta E_i^+ = \Delta E_i^\pm \pm e \sum_{j=1}^{N_p} q_j W^\parallel(z_j^\pm - z_i^\pm) \quad (16)$$

$$a_i^+ = a_i^\pm \pm \frac{e}{iE_0} \beta^{\frac{1}{2}} \sum_{j=1}^{N_p} q_j x_j^\pm W^\perp(z_j^\pm - z_i^\pm) \quad (17)$$

where  $x = \sqrt{\beta} \eta_i = \sqrt{\beta} \text{Re}[a_i(\theta) e^{iv_0\theta}]$

### 3.3 Acceleration

For acceleration by  $eV_a(z) = eV_c \sin\left(2\pi f_{rf} \frac{z}{c} + \phi_c\right)$ ,

$$\Delta E_i^+ = \Delta E_i^\pm + eV_c \sin\left(2\pi f_{rf} \frac{z_i^\pm}{c} + \phi_c\right) \quad (18)$$

$$a_i^+ = a_i^\pm \pm i \frac{eV_a^\pm}{E_0} \text{Im}[a_i^\pm e^{iv_0 u}] e^{\pm i v_0 u} \quad (19)$$

Eq.(25) is transverse radiation damping.

### 3.4 Radiation Excitation

$$\Delta E_i^+ = \Delta E_i^\pm + \sqrt{4 \frac{\Delta T}{\tau_E}} \left(\frac{\sigma_{E,0}}{E_0}\right) u_i \quad (20)$$

$$a_i^+ = a_i^\pm + \sqrt{4 \frac{\Delta T}{\tau_\beta} \epsilon_0} v_i e^{i 2\pi w_i} \quad (21)$$

where  $u$ ,  $v$  are the Gaussian random number and  $w$  is uniform random number.  $\Delta T$  is the time difference between each excitation and  $\tau_E$  and  $\tau_\beta$  is radiation damping time for  $E$  and  $x$ , respectively.  $\sigma_{E,0}$  and  $\epsilon_0$  are natural energy spread and emittance.

## 4. PARTICLE-IN-CELL METHOD

SISR is the particle code and a Particle-In-Cell(PIC) method is used to make wake field and interact the particle with the wake field. The shape function used in SISR is

$$S(x) = \begin{cases} \pm \left(\frac{x}{\Delta x}\right)^2 + \frac{3}{4} & (|x| \leq \frac{1}{2} \Delta x) \\ \frac{1}{2} \left|\frac{x}{\Delta x}\right|^2 \pm \frac{2}{3} & (\frac{1}{2} \Delta x \leq |x| \leq \frac{3}{2} \Delta x) \\ 0 & (\frac{3}{2} \Delta x \leq |x|) \end{cases} \quad (22)$$

and the distributions

$$\begin{pmatrix} \rho(z_p) \\ a\rho(z_p) \\ x\rho(z_p) \end{pmatrix} = \sum_{i=1}^N \begin{pmatrix} q_i \\ a_i q_i \\ x_i q_i \end{pmatrix} S(z_i \pm z_p) \quad (23)$$

are evaluated on the mesh points whose position is represented by  $z_p$ ,

And wake potentials appeared in above equations are evaluated at the mesh points using these distributions as

$$\begin{aligned} \frac{E_{BB}^\perp}{e}(z_p) &= \pm \sum_{j=1}^{N_p} q_j a_j \sum_{k=1}^{N_I} \beta_k W_k^\perp(z_j - z_p) \\ &= \pm \int a\rho(z') \sum_{k=1}^{N_I} \beta_k W_k^\perp(z' - z) dz' \end{aligned} \quad (24)$$

$$\begin{aligned} \frac{E_{local}^\perp}{e}(z_p) &= \pm \sum_{j=1}^{N_p} q_j x_j^\pm W^\perp(z_j^\pm - z_i^\pm) \\ &= \pm \int x\rho(z') W^\perp(z_j^\pm - z_i^\pm) dz' \end{aligned} \quad (25)$$

$$\begin{aligned} \frac{E^\parallel}{e}(z_p) &= \pm \sum_{j=1}^{N_p} q_j W^\parallel(z_j - z_p) \\ &= \pm \int \rho(z') W^\parallel(z' - z_p) dz' \end{aligned} \quad (26)$$

The wake potentials at the particles are obtained with

$$\frac{E}{e}(z_i) = \sum_{p=1}^{N_{mesh}} \frac{E}{e}(z_p) S(z_p \pm z_i) \quad (27)$$

## 5. WAKE FUNCTIONS

The three types of impedance models listed below are used to get wake functions. For longitudinal,

$Z^\parallel$	$\pm i \omega Z_L^\parallel$	$Z_R^\parallel$	$\frac{Z_C^\parallel}{\sqrt{\omega}} (1+i)$
$W^\parallel$	$Z_L^\parallel c^2 \frac{\partial \delta(z)}{\partial z}$	$Z_R^\parallel c \delta(z)$	$Z_C^\parallel \sqrt{\frac{2c}{\pi}}  z ^{\pm \frac{1}{2}} \theta(\pm z)$

and for transverse,

$Z^\perp$	$\pm i Z_L^\perp$	$\frac{Z_R^\perp}{\omega}$	$\frac{Z_C^\perp}{\omega \sqrt{\omega}} (1+i)$
$W^\perp$	$\pm Z_L^\perp c \delta(z)$	$\pm Z_R^\perp \theta(\pm z)$	$\pm Z_C^\perp 2\sqrt{\frac{2}{\pi c}}  z ^{\frac{1}{2}} \theta(\pm z)$

## 6. THE SPRING-8 STORAGE RING

The CISR is applied to the study of the instabilities of the SPring-8 storage ring. The parameters of the ring is shown in Table 1.

Table 1. The parameters of the SPring-8 storage ring.

Parameter		Value	Unit
Energy	$E_0$	8	GeV
Revolution Frequency	$T_0$	208.77	kHz
Energy Loss per Turn	$U_0$	9.2	MV
Damping Partition Numbers	$J_E / J_\beta$	2 / 1	
Momentum Compaction Factor	$\alpha$	$1.41 \times 10^{-4}$	
Betatron Tune (vertical)	$\nu_0$	16.16	
Averaged Betatron Function	$\beta$	17.3	m

The impedance of the ring is estimated in ref.[1] and is  $Z^\parallel = -1.67 \times 10^5 \omega i + 400 + 1.49 \times 10^8 \frac{1+i}{\sqrt{\omega}}$  (28)

$$Z^\perp = -2.13 \times 10^5 i + 4.98 \times 10^{14} + 4.21 \times 10^{10} \frac{1+i}{\omega \sqrt{\omega}} \quad (29)$$

where  $Z^\perp$  is vertical transverse impedance. The unit for them are  $\Omega$  and  $\Omega/\text{m}$ , respectively.

### 6.1 Longitudinal Instabilities

Figure 1 shows the dependence of the bunch length and the energy spread  $\sigma_E/E$  on the bunch current  $I_b$ . This ring is rather inductive compared with colliders, the potential-well distortion lengthen the bunch length and the threshold of microwave instabilities can not seen until the threshold current of the transverse instabilities mentioned later.

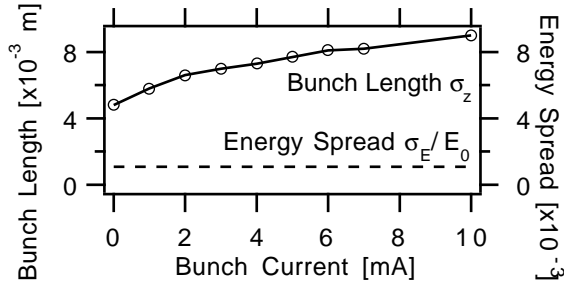


Figure 1. The bunch length and energy spread.

## 6.2 Transverse Instabilities

Figure 2 shows the bunch current increase vs. time used in the simulation.

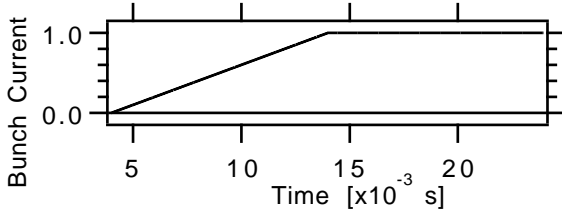


Figure 2. bunch current shape vs. time

Figure 3 and Figure 4 show the amplitude of betatron motion of the bunch vs. time for chromaticity  $\xi=0$  and  $\xi=4$ , respectively. Instabilities occur at  $I_b=3\text{mA}$  and  $I_b=7\text{mA}$  for  $\xi=0$  and  $I_b=10\text{mA}$  for  $\xi=4$ .

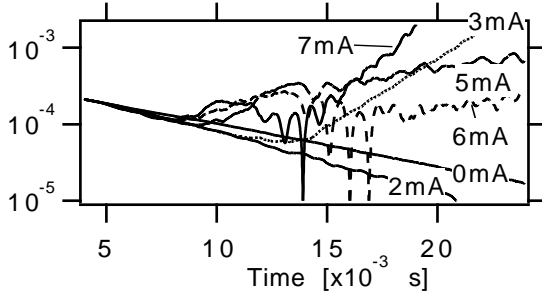


Figure 3. Amplitude of the betatron motion vs. time.  $\xi=0$ .

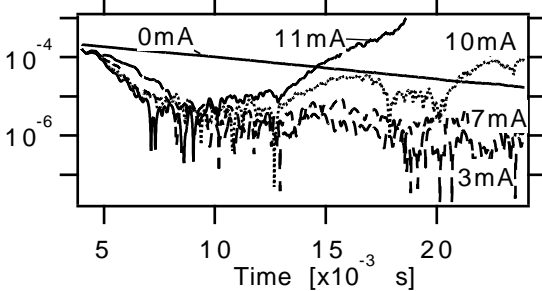


Figure 4. amplitude of the betatron motion vs. time.  $\xi=4$ .

Figure 5 and 6 are the spectrum of the betatron motion of the bunch.  $(m,n)=(0,0)$  and  $(m,n)=(0,1)$  mode can be seen. The  $m=1$  mode must exist at the synchrotron frequency  $f_s=1.5\text{kHz}$  lower position, around  $f=32\text{kHz}$ , but no signal can be seen.

From Figure 5, which is for  $\xi=0$ , the coupling of mode  $(m,n)=(0,0)$  and  $(m,n)=(1,0)$  occurs at  $I_b=3\text{mA}$  and the coupling of mode  $(m,n)=(0,0)$  and  $(m,n)=(2,0)$  occurs at  $I_b=7\text{mA}$ . Both lead to instabilities. For chromaticity  $\xi=4$ , of

which data is not shown here, the signal of mode  $(m,n)=(0,0)$  can not be seen.

In Figure 4, No instabilities occurs near  $I_b=3\text{mA}$ , but the  $m=2$  mode grows up at  $I_b=10\text{mA}$ . The difference between  $\xi=0$  and  $\xi=4$  seems to be from the effect of the head-tail damping, which can be seen at the beginning of the bunch current increase, where time  $\sim 5\text{ms}$  in Figure 4 and it is faster than radiation damping time which is seen for  $I_b=0\text{mA}$ .

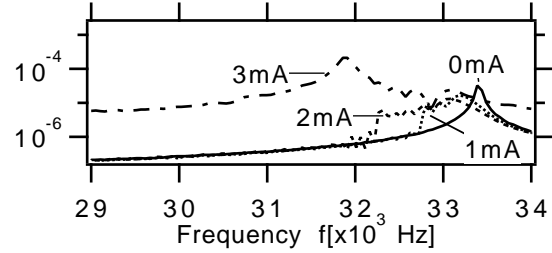


Figure 5. Spectrum of the betatron motion of the bunch,  $I_b=0\text{mA}, 1\text{mA}, 2\text{mA}, 3\text{mA}$ .  $\xi=0$ .

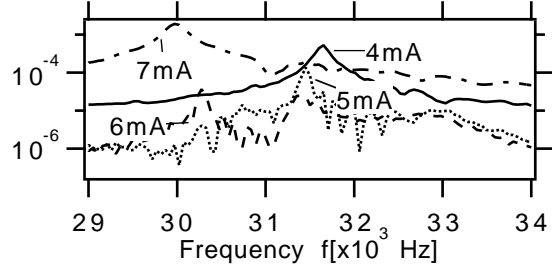


Figure 6. Spectrum of the betatron motion of the bunch,  $I_b=4\text{mA}, 5\text{mA}, 6\text{mA}, 7\text{mA}$ .  $\xi=0$ .

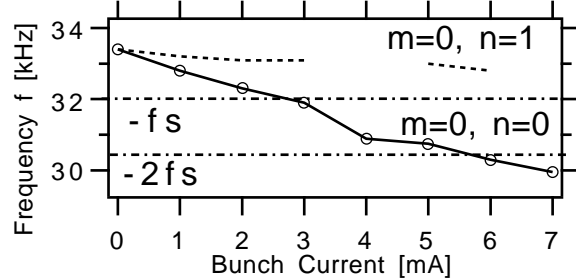


Figure 7. The position of peak of each mode of the spectrum of the betatron motion of the bunch.  $\xi=0$ .

When chromaticity  $\xi=-2$ , the growth-rate of the head-tail mode of  $m=0$  is so high and the threshold current is around few tenth mA.

## 7. CONCLUSION

The simulation code for single-bunch instabilities was developed and applied to the SPring-8 storage ring. No longitudinal microwave instabilities can not be seen and the threshold of the transverse instabilities is a few mA and the positive chromaticity increase the threshold current.

## 8. REFERENCES

- [1] T. Nakamura, "ESTIMATION OF LONGITUDINAL AND TRANSVERSE IMPEDANCE OF THE SPRING-8 STORAGE RING," this conference.